Ultrasound induced fragmentation of primary Al₃Zr crystals

Abhinav Priyadarshi[1,*], *Tungky* Subroto[2], *Marcello* Conte[3], *Paul* Prentice[4], *Koulis* Pericleous[5], *Dmitry* Eskin[2,6], *John* Durodola[1], and *Iakovos* Tzanakis[1,7]

[1] Faculty of Technology, Design and Environment, Oxford Brookes University, Oxford OX33 1HX, United Kingdom
[2] Brunel Centre for Advance Solidification Technology (BCAST), Brunel University London, Uxbridge UB8 3PH, United Kingdom
[3] Anton Paar TriTec SA, Vernets 6, 2035 Corcelles, Switzerland
[4] Cavitation Laboratory, School of Engineering, University of Glasgow, Glasgow G12 8QQ, United Kingdom
[5] Computational Science and Engineering Group (CSEG), Department of Mathematics, University of Greenwich, London SE10 9LS, United Kingdom
[6] Tomsk State University, Tomsk 634050, Russia
[7] Department of Materials, University of Oxford, Oxford OX1 3PH, United Kingdom

Abstract. Ultrasonic cavitation melt treatment (UST) of aluminium alloys has received considerable attention in the metal industry due to its simple and effective processing response. The refined primary intermetallic phases formed in the treated alloys during controlled solidification, govern alloy structural and mechanical properties for applications in the automotive and aerospace industries. Since the UST is performed close to the liquidus temperatures of the alloys, understanding the refinement mechanism of the primary intermetallic phases has been beset by difficulties in imaging and handling of liquid metals. In this paper, the sonofragmentation behaviour of primary intermetallic Al₃Zr crystals extracted from the matrix of an Al-3 wt% Zr alloy and fixed on a solid substrate was investigated. The intermetallics were exposed to cavitation action in deionized water at 24 kHz of ultrasound frequency. The fragmentation mechanism from the nearby collapsing cavitation bubbles was studied with in-situ high speed imaging. Results revealed that the main fragmentation mechanism is associated with the propagation of shock wave emissions from the collapsing bubble clouds in the vicinity of the crystal. The mechanical properties of the Al₃Zr phase determined previously were used for the fracture analysis. It was found that an Al₃Zr intermetallic undergoes low cycle fatigue fracture due to the continuous interaction with the shock wave pressure. The magnitude of the resulting shear stress that leads to intermetallic fragmentation was found to be in the range of 0.6 – 1 MPa.

Keywords: Ultrasonic melt treatment, intermetallic crystal, high speed imaging, cavitation, fragmentation, deflection

1 Introduction

Ultrasound induced cavitation and its possible benefits in liquid metal processing has received considerable attention from both the academic and industrial communities since the 1950's. Ultrasonic melt treatment (UST) being an eco-friendly, sustainable and economical processing route offers several advantages in terms of degassing, enhanced heterogeneous nucleation and structural refinement of the as-cast product resulting in improved quality of the material [1,2].

Primary intermetallics of finer size and shape formed in the Al alloys are highly desirable to augment heterogeneous nucleation in the alloy melt during solidification and so obtain microstructural refinement leading to enhancements in mechanical properties. Although induced ultrasonic cavitation in metallic melts

has been proven to be the cause of structural refinement of various Al alloys [3], the fundamental understanding of the mechanism by which UST promotes fragmentation and the corresponding nucleating effects to obtain finer grain structures is still deficient. Previously the effects of UST in light alloy melts have only been studied using ex-situ (i.e. after the treatment) characterization techniques to analyse the ultrasonically treated materials. In recent years, in-situ characterization methods have received much attention for UST performance visualization in real time conditions [4–8]. The two most common in-situ experimental techniques for characterizing materials processed using UST are; (i) high-speed optical imaging of transparent organic liquids/melts, and (ii) X-ray synchrotron radiography of liquid metals. The former technique is much more widely established due to low temperature processing

---

* Corresponding author: abhinav.priyadarshi-2018@brookes.ac.uk

and transparent nature of the treated samples. The latter technique allow the real time observation of the cavitation bubbles and corresponding phenomena specifically growth rate, average radius and their distribution. However, due to handling and processing difficulties of analysing real metallic melts and limited field of view for capturing the dynamic effects of multi-phase interactions, a common technique is to use optically transparent liquids such as water to replicate the cavitation conditions and monitor the interaction with the solid phases during treatment. In-situ optical imaging studies of solidifying organic transparent alloys under the presence of ultrasound have proven to be effective for analysing grain nucleation by fragmentation of evolving dendritic structures accelerated by the oscillation of stable and transient cavitation bubbles [4,6]. Specifically, Shu et al. [5] found that the rate of fragmentation of growing dendrites in transparent organic alloy systems can be either slow or violent and depends primarily on the type of cavitation bubbles. Lately, in-situ synchrotron X-ray imaging has also been applied to studying real liquid metals under the influence of different external fields [9–11]. Growth rate, average radius and distribution of cavitation bubble sizes in Al-10 wt% Cu alloy was studied by Xu et al. [9] and Mi et al. [12]. Tzanakis et al. [13] provided the first direct evidence of instantaneous re-filling of a micro-capillary channel using Al-10 wt% Cu alloy melt confirming the previously postulated ultrasonic capillary effect (UCE). Dynamic collapse of a cavitation bubble in multiphase liquid flow in a Bi-8 wt% alloy melt has been observed by Tan et al. [14]. Although, observation of cavitation bubbles and their dynamic behaviour under the influence of ultrasound in real and transparent organic melts have been conclusive to a certain extent, understanding of the direct interaction of ultrasound with the dispersed or agglomerated solid phase is still lacking. Wagterveld et al. [15] imaged the influence of acoustic cavitation on suspended calcite crystals in saturated $CaCO_3$ solution and demonstrated that fracture of single calcite crystals is induced by the inception and collapse of cavitation cluster and acoustic streaming. Wang et al. [16] noticed that the fracture of intermetallics by the action of nearby cavitation bubbles is not an instantaneous process and requires substantial time to occur. In addition to handling and processing difficulties in analysing real metallic melts through in-situ X-ray synchrotron technique, the radiography method offers a very limited field of view for capturing the dynamic effects of multi-phase interactions.

In this paper, following an approach used by Wang et al. [16] the cavitation-induced fragmentation of extracted primary Al_3Zr crystals under the influence of a 24 kHz ultrasonic excitation signal has been investigated in deionized water by high-speed imaging. The fracture mechanism of a single intermetallic crystal has been elucidated using the recorded images and the stress-deflection theory. The induced stress has also been compared with the crack propagation studies conducted earlier.

2 Methodology

2.1 Sample preparation

Pure Al and a master alloy (Al-5wt% Zr) were smelted to produce about 350 grams of an Al-3wt% Zr alloy. The cast alloy was then re-melted using an electric arc furnace and slowly cooled in a cylindrical graphite crucible of 50 mm diameter following a thermal cycle as discussed in [17]. Al-3wt.% Zr alloy cubes of dimension 5 x 5 x 5 mm were cut from the solidified ingot using a rotating silicon carbide blade.

Extraction of the primary Al_3Zr crystals was done by immersing the alloy in a 15% NaOH water solution for 24 hrs. Subsequently, the Al matrix was completely dissolved leaving only the primary crystals based on the following chemical reaction:

$$2Al + 2NaOH + 2H_2O \rightarrow 2NaAlO_4 + 3H_2$$
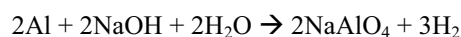
The intermetallic crystals were then filtered out from the solution and were carefully rinsed with ethanol and left to dry out prior to the sonofragmentation studies. The optical micrographs of an Al-3wt% Zr alloy and extracted Al_3Zr intermetallic particles are displayed in Fig. 1.
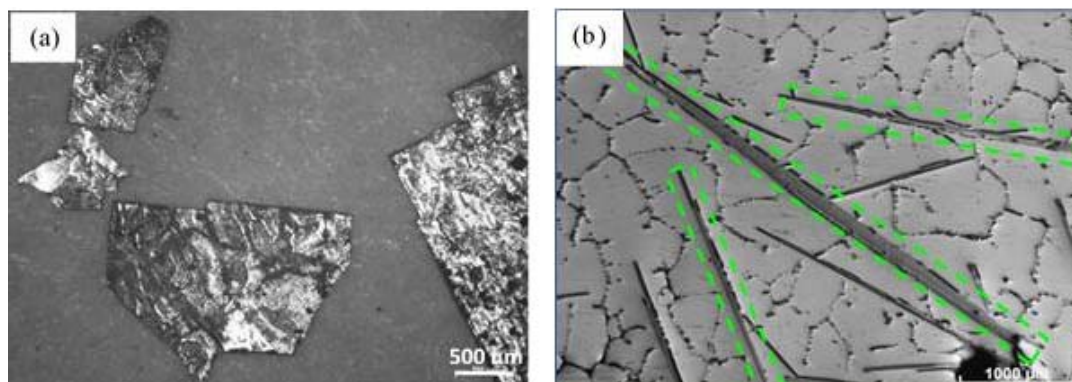
Fig. 1. Morphological images of Al_3Zr (a) extracted crystals, (b) intermetallics embedded (highlighted in green) in Al-3wt%Zr alloy matrix.

2.2 Experimental setup

The chemically extracted intermetallic particles were fixed on a steel base with a superglue adhesive and placed in a glass container of dimension 7.5 cm x 7.5 cm x 10 cm. The intermetallic was strategically positioned 2-3 mm below the piezoelectric transducer with a titanium sonotrode tip of 3 mm diameter with power density of 460 W/cm^2 (Hielscher UP200S processor) operating at a frequency of 24 kHz. The UP200S ultrasonic processor handbook enlists the detailed configuration of the system [18]. The ultrasound excitation was employed at a selected amplitude of 210 µm and the experiments were conducted in de-ionized water at room temperature.

Before capturing the fragmentation phenomenon, monitoring of the cavitation field just below the sonotrode tip and within 2 mm distance where the intermetallic crystals were later mounted was performed using a Hyper Vision HPV X2 (Shimadzu, Japan) high speed video camera and images were recorded at 1M fps in order to capture the fast shock wave propagation from the collapsing bubbles under synchronous 10 ns laser pulse illumination as in [19]. A In-situ interaction of intermetallic particles and ultrasound induced cavitation was filmed using a high-speed camera (Photron SA-Z) operating at 100,000 fps adequate to capture the fragmentation sequence of intermetallics. The camera lens was placed at a distance of 165 mm from the ultrasound source to have a full focussed observation of the interaction plane. For imaging with maximum illumination of the interaction plane, a multi LED flash light (GS Vitec) was used illuminating both the front and rear of the tank. The schematic of the experimental setup is illustrated in Fig. 2.
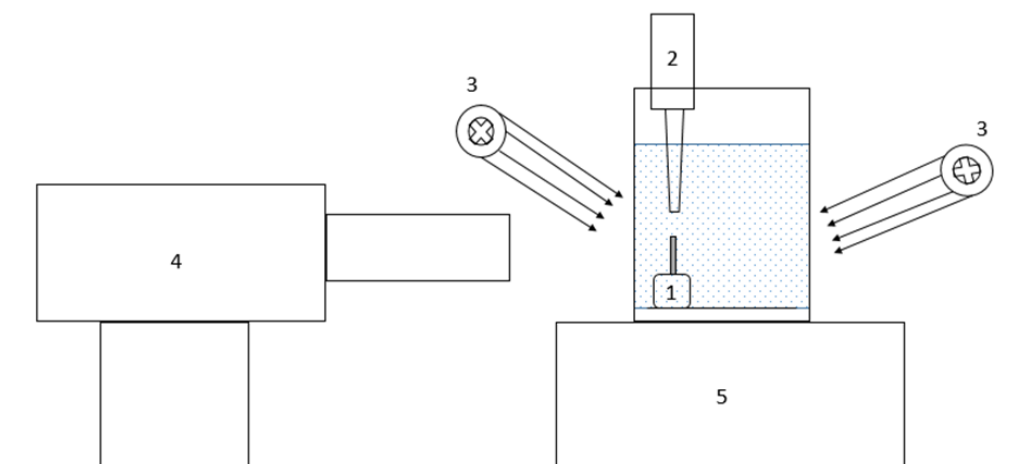
Fig. 2. A schematic of the in-situ high-speed imaging setup involving, (1) extracted Al$_3$Zr intermetallic, (2) ultrasonic processor with horn, (3) LED flash lamp, (4) high speed camera, and (5) movable platform.
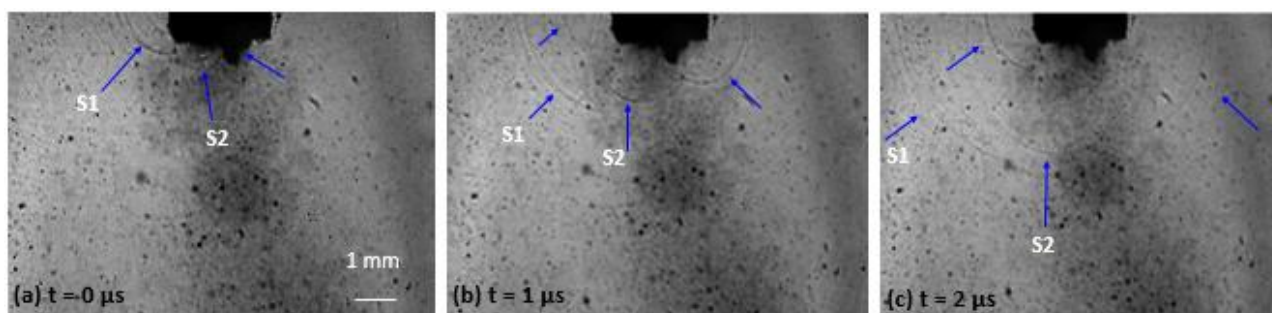
Fig. 3. Representative high-speed images of ultrasound induced cavitation and emitted shock waves recorded at 1M fps.

3 Results and discussion

3.1 Ultrasonic cavitation and shock wave emission

Figure 3 shows recorded images of ultrasound induced cavitation cloud and propagating shock wave fronts from the imploding bubbles. From the sequence of images, it is evident that introduction of an ultrasonic wave in a liquid medium leads to the development of acoustic cavitation cloud and emission of periodic high energy shock waves reaching pressures of several GPa and shock velocities up to 4000 m/s [20,21]. However, most of the shock wave energy is released within the first few hundred micrometres from the bubble rim [21]. Fig. 3(a-c) represents the movement of shock waves marked as S1 and S2 (indicated with blue curves and arrows) at definite intervals. It can be seen from the images that as the shock wave S1 propagates further away, another shock wave emerges from a thick cavitation cloud near the ultrasonic horn and the progression continues. Using frame by frame images, the velocity of S1 was calculated at a radial distance of approximately 3 mm and was found out to be almost 1650 m/s. It has been frequently observed that these emitted shock wave are responsible for micro-damage on any solid surface present in their vicinity [22]. Other effects such as micro-streaming and turbulences have also been found to attack the solid interfaces aggressively causing fragmentation and erosion of the material [23].

3.2 Fragmentation of primary Al$_3$Zr particles

To better understand and observe the effect of shock wave fronts on the fragmentation of the intermetallic crystals, the imaging was carried out at a comparatively lower frame rate i.e. 100000 fps Figure 4(a-l) represents the fragmentation sequence of the two Al$_3$Zr crystals, one placed in a perpendicular plane to the other. The displayed sequences of fragmentation images are representative of at least 10 of similar and reproducible observations. Only carefully chosen images haven been included for brevity of the manuscript. The first frame at *t = 0 μs*, shows the two crystals positioned at right angles to each other. From here onwards, the crystal on the left will be referred to as side facing (SF) crystals and the crystal on the right will be mentioned as front facing (FF) crystal to avoid any ambiguity for the reader. Figure 4a shows the two well developed and illuminated tabular-plated crystals with similar dimensions; roughly 3 mm x 2.5 mm and a thickness of 60 - 100 μm. The detailed morphology of these primary Al$_3$Zr crystals can be found elsewhere [24]. The first frame also shows the SF crystal having a small notch on the edge (marked in red). It should be noted that the visibility and details of

the notch/crack are limited by the camera resolution based on the present high-speed images. The ultrasonic device was subsequently switched on generating a cluster of cavitating bubbles across the sonotrode tip as depicted in Fig. 4b. As soon as the bubble cloud starts to propagate towards the crystal, slight deflection of the tip of SF is observed (marked in yellow). Since this sequence of images was recorded using white light illumination, it was difficult to capture the propagation of shock waves due to wavelength restrictions. After about 4 ms, the SF crystal above the small notch (indicated with the arrow mark) starts to deflect vigorously due to continuous emission of shock waves from the oscillating and imploding bubble cloud. At the same time, a fine crack was also formed on the FF crystal (marked in red). With the continuous oscillation of the ultrasonic horn tip, the cavitation cloud became bigger, simultaneously moving towards the crystal causing both the notch and crack to enlarge and grow in size [Fig. 4(e-f)] until it completely separated off the parent crystal (Fig. 4g). Note that up till this period the cavitation cloud had not even reached those locations of crystal imperfections from where the notch/crack began to grow indicating that shock waves (reaching ahead of the cloud) have the potential to fragment the intermetallic crystals rapidly and violently. It is also important to understand that the occurrence of the notches/cracks in the crystal results from geometrical irregularities structural defects and micro-cracks arising from the residual stresses in the intermetallic. It is also interesting to note that once the crack initiates and reaches its critical length, the crystal fails immediately in just 270 μs confirming the extremely brittle nature of the intermetallic as observed by authors in [25]. It was also revealed that the shock waves emitted from the collapse of a single cavitation bubble are primarily responsible for the fragmentation of the solid interface present nearby. At around *t = 10 ms,* the cavitation field further grows and encapsulates half of the crystal (SF and FF). Figure 4i shows the real time snapshot of the maximum deflection induced in the SF crystal (marked in yellow). With a continued oscillating cavitation field, the SF crystal experienced cyclic fatigue owing to developed shear stresses before completely fragmenting at *t = 12.42 ms* as shown in Fig. 4j. At the same instant, a crack can be seen on FF crystal (marked with red arrow) which also eventually propagates and breaks off (Fig. 4k). Overall, this whole process of intermetallic failure can be attributed to the combined effect of cavitation bubble collapses and emitted shock waves. From the sequence of high speed images, it can also be deduced that the first fracture happens in just 86 cycles of ultrasonic vibrations representative of low cycle fatigue failure. The crystal disintegrates into micron sized particles in few acoustic cycles upon sonofragmentation

---

*
  Corresponding author: abhinav.priyadarshi-2018@brookes.ac.uk
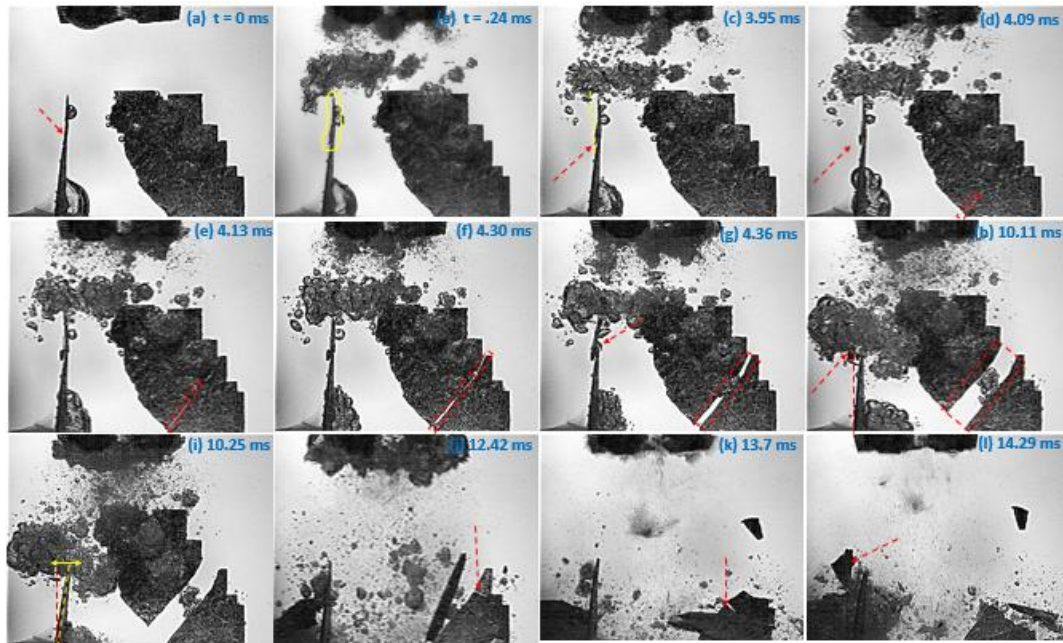
Fig. 4. Real-time high-speed photographic sequence capturing ultrasound induced fragmentation of Al$_3$Zr intermetallic crystal at 100,000 fps.

3.3 Application of stress-deflection theory

It has been previously observed that for an intermetallic crystal with a pre-existing notch/crack to fail completely, the required tensile stress should be in the range of 20-30 MPa and the shock pressure amplitude generated from a single (laser-induced) bubble is around 30-40 MPa at a distance of 2-3 mm [25]. However, in the case of ultrasound, the pressure amplitude of the induced cavitation field is expected to be strongly reduced owing to decrease in acoustic radiation resistance (real part of acoustic radiation impedance) [26]. The acoustic pressure was measured at a distance of 2 mm (the position of the intermetallic crystal from the sonotrode surface) using a calibrated fibre optic hydrophone system and was found to be around 1 ± 0.2 MPa.

The reason for this relatively low value of pressure compared to the pressure obtained from the single bubble collapse [25] can be attributed to the cavitation shielding [27] and the decrease in the speed of sound and the density of the surrounding medium due to the presence of bubble clouds under the sonotrode as observed by Yasui et al. [26].

In order to determine the magnitude of the shear stress acting on the tip of SF crystal (Fig. 4i), the crystal was considered to be a rectangular plate cantilever of length *L*, width, *b* and thickness *d*, as illustrated in Fig. 5 for the sake of geometrical simplicity. The maximum shear stress was mathematically evaluated based on the deflection observed from the frame by frame high speed images and the corresponding pixel size using the following equation [28]:

$$\tau_{max} = \frac{FQ}{Ib} \tag{1}$$

where, *F* is the transverse shear force obtained from the maximum deflection (δ_{max}) of the cantilever, *Q* is the first moment of area, *I* is the moment of inertia and *b* is the width of the crystal. For the stress calculation, the elastic modulus (E) of Al$_3$Zr crystal was taken from previously conducted nanoindentation measurements as 200 GPa [25].

---

* Corresponding author: abhinav.priyadarshi-2018@brookes.ac.uk

$$F = \frac{3\delta_{max}EI}{L^3}$$

$$Q_{z-z'} = \frac{bd^2}{8}$$

$$I = \frac{bd^3}{12}$$
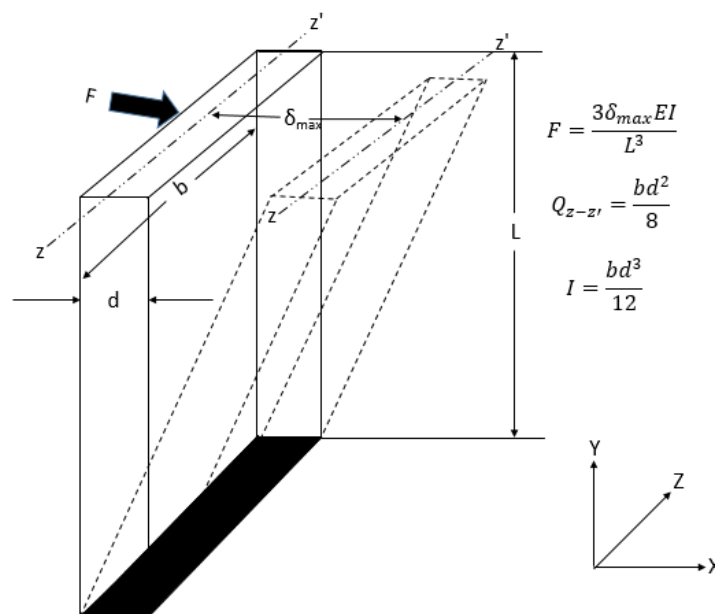
Fig. 5. Schematic of one end fixed crystal acted upon by transverse shear force F.

Using Eq. 1, and assuming that the maximum shear force is acting exactly on the tip of the crystal, the corresponding maximum shear stress produced on the intermetallic is estimated to be about 0.77 MPa while the measured cyclic acoustic pressure at that location was found to be slightly higher inducing low cycle fatigue within the intermetallic leading to fragmentation. The shear stress developed at the tip of the crystal was confirmed after 10 such observations and the average stress was found to be 0.8 ± 0.2 MPa. Nevertheless, this approximation was established for a constant load, which is not illustrative of the influence of continuous pressure pulses generated by the shock front on the crystal. Moreover, the acoustic pressure generated by the ultrasound induced cavitation bubbles cannot elucidate the fragmentation alone. Additional effects of pulsating cavitation bubbles on the crystal surface, effect of shock waves released and the liquid jet upon collapse, also need to be considered, accelerating the fragmentation.

4 Conclusions

Sonofragmentation experiments of primary Al_3Zr intermetallic crystals extracted from an Al-3wt.% Zr alloy were conducted in water. The fracture mechanism was elucidated using in-situ high speed imaging. The shock wave induced stress on the crystal was quantified using the defection fracture mechanics approach. It was confirmed that the high energy shock wave resulting from cavitation bubble collapse is mainly responsible for the fragmentation of the crystal. The Al_3Zr intermetallic undergoes cyclic deflection and eventually fails in a typical brittle manner upon interaction with the propagating shock front and cavitation bubble clouds. Crystal failure occurs in 80-100 acoustic cycles implying a low cycle fatigue fracture mechanism. The acoustic pressure amplitude at a distance of approximately 3 mm was found to be approximately 1 MPa, which is sufficient for fragmenting an intermetallic present nearby.

References

1. O. V. Abramov, *High-Intensity Ultrasonics : Theory and Industrial Applications* (Gordon and Breach Science Publishers, Amsterdam, The Netherlands, 1998).

2. G. I. Ėskin and D. G. Eskin, *Ultrasonic Treatment of Light Alloy Melts* (CRC Press, Boca Raton, Florida, 2015).

3. G. I. Eskin, Ultrason. Sonochem. **8**, 319 (2001).

4. G. M. Swallowe, J. E. Field, C. S. Rees, and A. Duckworth, Acta Metall. **37**, 961 (1989).

5. D. Shu, B. Sun, J. Mi, and P. S. Grant, Metall. Mater. Trans. A **43**, 3755 (2012).

6. R. Chow, R. Blindt, A. Kamp, P. Grocutt, and R. Chivers, Ultrason. Sonochem. **11**, 245 (2004).

7. W. W. Xu, I. Tzanakis, P. Srirangam, S. Terzi, W. U. Mirihanage, D. G. Eskin, R. H. Mathiesen, A. P. Horsfield, and P. D. Lee, (Springer International Publishing, Cham, 2015), pp. 61–66.

Corresponding author: abhinav.priyadarshi-2018@brookes.ac.uk

8. I. Tzanakis, W. W. Xu, G. S. B. Lebon, D. G. Eskin, K. Pericleous, and P. D. Lee, Phys. Procedia **70**, 841 (2015).

9. W. W. Xu, I. Tzanakis, P. Srirangam, W. U. Mirihanage, D. G. Eskin, A. J. Bodey, and P. D. Lee, Ultrason. Sonochem. **31**, 355 (2016).

10. E. Liotti, A. Lui, R. Vincent, S. Kumar, Z. Guo, T. Connolley, I. P. Dolbnya, M. Hart, L. Arnberg, R. H. Mathiesen, and P. S. Grant, Acta Mater. **70**, 228 (2014).

11. D. Ruvalcaba, R. H. Mathiesen, D. G. Eskin, L. Arnberg, and L. Katgerman, Acta Mater. **55**, 4287 (2007).

12. J. Mi, D. Tan, and T. L. Lee, Metall. Mater. Trans. B Process Metall. Mater. Process. Sci. **46**, 1615 (2015).

13. I. Tzanakis, W. W. Xu, D. G. Eskin, P. D. Lee, and N. Kotsovinos, Ultrason. Sonochem. **27**, 72 (2015).

14. D. Tan, T. L. Lee, J. C. Khong, T. Connolley, K. Fezzaa, and J. Mi, Metall. Mater. Trans. A Phys. Metall. Mater. Sci. **46**, 2851 (2015).

15. R. M. Wagterveld, L. Boels, M. J. Mayer, and G. J. Witkamp, Ultrason. Sonochem. **18**, 216 (2011).

16. F. Wang, I. Tzanakis, D. Eskin, J. Mi, and T. Connolley, Ultrason. Sonochem. **39**, 66 (2017).

17. A. Priyadarshi, T. Subroto, M. Conte, K. Pericelous, D. Eskin, P. Prentice, and I. Tzanakis, in *Miner. Met. Mater. Ser.* (Springer, 2020), pp. 168–173.

18. "Instruction manual UP200S/ UP400s," *Hielscher*, 2007.http://www.bendarygroup.com/images/instruction_manual_up200_400s_2007_ultrasonics.pdf.

19. K. Johansen, J. H. Song, K. Johnston, and P. Prentice, Ultrasonics **73**, 144 (2017).

20. R. Pecha and B. Gompf, Phys. Rev. Lett. **84**, 1328 (2000).

21. E. A. Brujan, T. Ikeda, and Y. Matsumoto, Exp. Therm. Fluid Sci. **32**, 1188 (2008).

22. T. Prozorov, R. Prozorov, and K. S. Suslick, J. Am. Chem. Soc. **126**, 13890 (2004).

23. K. S. Suslick and G. J. Price, Annu. Rev. Mater. Sci. **29**, 295 (1999).

24. S. Zhen and G. J. Davies, J. Cryst. Growth **64**, 407 (1983).

25. K. Yasui, Y. Iida, T. Tuziuti, T. Kozuka, and A. Towata, Phys. Rev. E - Stat. Nonlinear, Soft Matter Phys. **77**, (2008).

26. G. S. B. Lebon, I. Tzanakis, K. Pericleous, and D. Eskin, Ultrason. Sonochem. **42**, 411 (2018).

27. J. M. Gere and B. J. Goodno, *Mechanics of Materials* (Cengage Learning, 2013).